ARMY RESEARCH LABORATORY

Surface Enhanced Raman Scattering (SERS) Detection of Ammonium Nitrate (AN) Samples Fabricated Using Drop-on-Demand Inkjet Technology on Commercial and Fabricated SERS Substrates

by Mikella E. Farrell, Ellen L. Holthoff, and Paul M. Pellegrino

ARL-TR-6424 **April 2013**

NOTICES

Disclaimers

The findings in this report are not to be construed as an official Department of the Army position unless so designated by other authorized documents.

Citation of manufacturer's or trade names does not constitute an official endorsement or approval of the use thereof.

Destroy this report when it is no longer needed. Do not return it to the originator.

Army Research Laboratory
Adelphi, MD 20783-1197

ARL-TR-6424 **April 2013**

Surface Enhanced Raman Scattering (SERS) Detection of Ammonium Nitrate (AN) Samples Fabricated Using Drop-on-Demand Inkjet Technology on Commercial and Fabricated SERS Substrates

Mikella E. Farrell, Ellen L. Holthoff, and Paul M. Pellegrino
Sensors and Electron Devices Directorate, ARL

REPORT DOCUMENTATION PAGE

Form Approved
OMB No. 0704-0188

1. **REPORT DATE** *(DD-MM-YYYY)*	**2. REPORT TYPE**	**3. DATES COVERED (From - To)**
April 2013	Final	

4. TITLE AND SUBTITLE
Surface Enhanced Raman Scattering (SERS) Detection of Ammonium Nitrate (AN) Samples Fabricated Using Drop-on-Demand Inkjet Technology on Commercial and Fabricated SERS Substrates

5a. CONTRACT NUMBER

5b. GRANT NUMBER

5c. PROGRAM ELEMENT NUMBER

6. AUTHOR(S)
Mikella E. Farrell, Ellen L. Holthoff, and Paul M. Pellegrino

5d. PROJECT NUMBER

5e. TASK NUMBER

5f. WORK UNIT NUMBER

7. PERFORMING ORGANIZATION NAME(S) AND ADDRESS(ES)
U.S. Army Research Laboratory
ATTN: RDRL-SEE-E
2800 Powder Mill Road
Adelphi, MD 20783-1197

8. PERFORMING ORGANIZATION REPORT NUMBER
ARL-TR-6424

9. SPONSORING/MONITORING AGENCY NAME(S) AND ADDRESS(ES)

10. SPONSOR/MONITOR'S ACRONYM(S)

11. SPONSOR/MONITOR'S REPORT NUMBER(S)

12. DISTRIBUTION/AVAILABILITY STATEMENT
Approved for public release; distribution unlimited,

13. SUPPLEMENTARY NOTES
mikella.e.farrell.civ@mail.mil

14. ABSTRACT
The U.S. Army and first responder community are increasingly focusing efforts on energetic materials detection and identification. Main hazards encountered in theater include homemade explosives (HMEs) and improvised explosive devices (IEDs), in part fabricated from simple components like ammonium nitrate (AN). In order to accurately detect and identify these unknowns (energetic or benign), fielded detection systems must be accurately trained using well-understood universal testing substrates. These training substrates must contain target species at known concentrations and recognized polymorphic phases. AN is an explosive precursor material that demonstrates several different polymorphic phases depending on how the material is deposited onto testing substrates. In this report, known concentrations of AN were uniformly deposited onto commercially available surface enhanced Raman scattering (SERS) substrates using a drop-on-demand inkjet printing system. The phase changes observed after the deposition of AN under several solvent conditions are investigated. Characteristics of the collected SERS spectra of AN are discussed and it is demonstrated that an understanding of the exact nature of the AN samples deposited results in an increased ability to accurately and reliably "train" hazard detection systems.

15. SUBJECT TERMS
Raman, SERS, ammonium nitrate, drop-on-demand

16. SECURITY CLASSIFICATION OF:			**17. LIMITATION OF ABSTRACT**	**18. NUMBER OF PAGES**	**19a. NAME OF RESPONSIBLE PERSON**
a. REPORT	**b. ABSTRACT**	**c. THIS PAGE**			Mikella E. Farrell
Unclassified	Unclassified	Unclassified	UU	32	**19b. TELEPHONE NUMBER** (*Include area code*) (301) 394-0948

Standard Form 298 (Rev. 8/98)
Prescribed by ANSI Std. Z39.18

Contents

List of Figures

1. Introduction

1.1 Objective

Sensitive, accurate, and reliable methods are needed to detect and identify chemical explosive hazards. An analyte of particular interest to the U.S. Army and first responder community is ammonium nitrate (AN). This material has many practical applications in agriculture; however, it is also extensively used in the manufacture of industrial explosives. Unfortunately, it is also becoming a regularly used component of fertilizer bombs or improvised explosive devices (IEDs) seen throughout the world. One tragic example of terrorist use of AN occurred in the attack in the U.S. in 1995 with the bombing of the Alfred P. Murrah Federal Building in downtown Oklahoma City (*1*). Since then, the use of AN by terrorist groups and the resulting devastation from material detonation, has continued to challenge military and law enforcement personnel both at home and abroad. In 2012, USA Today reported (*2*) that in Afghanistan the "number of improvised explosive devices that were cleared or detonated rose to 16,554 from 15,225, an increase of 9%." With the evident increase in IEDs and easily obtained and prevalent supply of AN in agricultural areas, the U.S. Army and first responder community are increasingly focusing efforts on energetic materials detection and identification (*3–11*). To combat this growing threat, several optically based hazard detection systems are being evaluated for fielded applications aiming to provide rapid detection and identification of bulk and trace concentrations of hazardous materials (*12*).

Of the many available techniques researched for energetic and hazardous materials detection, Raman and Raman-based technologies are gaining attention (*13–27*). These techniques are increasingly being used to address the outstanding need and challenge for rapid sensitive and accurate detection, identification, and quantification of chemical, biological, and energetic hazards in many fields of interest (e.g., medical, environmental, industrial, and defense applications) (*28*). In particular, there has been a push to detect trace levels of hazardous materials left behind on common items like hair, clothes, and even fingerprints (*29–34*). One Raman-based detection method that is gaining significant popularity for meeting these sensitivity needs is surface enhanced Raman scattering (SERS) (*35–37*).

1.2 Surface Enhanced Raman Scattering (SERS)

SERS-based techniques and platforms combine traditional spectroscopy with trace level detection capabilities. SERS is a particularly advantageous and appropriate hazard detection technique as it does not suffer from interferences from water, requires little to no sample preparation, is robust and can be used in numerous environments, is relatively insensitive to the wavelength of excitation employed, and produces a narrowband spectral signature unique to the

molecular vibrations of the analyte. Since the discovery of SERS in the 1970s, it has been experimentally shown that, compared to spontaneous Raman, SERS signal enhancements of up to 14 orders of magnitude are observed on metalized (typically silver or gold) nanoscale roughened surfaces (*38–41*).

Because of the many sensing advantages of SERS-based techniques, significant research efforts have been directed toward developing SERS substrates for SERS-based sensor platforms (*42–51*). There are numerous examples in the literature on how varying the substrate architecture (e.g., geometry, feature spacing and height, metal used) can result in very dramatic changes to the overall SERS enhancing capabilities of the substrate surface. Furthermore, research (university and industry) continues to push towards the development of a uniform, reproducible, mass-produced product necessary to facilitate widespread incorporation of SERS in viable sensing platforms. An example of a fabricated SERS substrate was investigated under a Presidential Early Career Award for Scientists and Engineers (PECASE) Army Research Office (ARO) award W911NF-09-1-0101. These substrates have been previously described (*52–54*). Generally, these substrates are fabricated using a simple one-step direct imprinting process, thus, creating a porous gold grating film that has previously been shown to contribute to a SERS enhancement (*54*). Some success fabricating both spectrally and physically reproducible SERS substrates has been demonstrated with commercially available standard Klarite® substrates (Renishaw Diagnostics) (*55–59*). These substrates were developed using silicon-based semiconductor fabrication techniques (*59*). Klarite substrates consist of an array of highly reproducible inverted pyramid features (*59*), which have "hot spots" or "trapped plasmons" located inside the wells (*59*). Such substrates have been previously characterized (*60*).

1.3 Polymorphic Phase Material

In the current work, AN is uniformly deposited onto both standard commercial and fabricated SERS substrates using a standardized drop-on-demand inkjet methodology demonstrated at the U.S. Army Research Laboratory (ARL) (*61*). AN is an important fertilizer and has also shown to be a powerful component of homemade explosives (HMEs) and IEDs. Therefore, a great deal of research has been focused on better understanding not only its kinetic properties, but also means of detecting this material. It has been shown that when sample concentrations are deposited on a surface, in some cases, the polymorphic state of a material can be altered by the solvent deposition process or even the analyte pretreatment steps (*61*). Specifically, when a material can exist in multiple polymorphic phases, the phase that is formed after solvent evaporation can depend on factors such as the nature of the particular solvent used, the concentration of the deposited solution, the evaporation rate of the solvent, the substrate surface structure onto which the material is deposited, or even the heating and cooling cycles employed during drying (*62*). AN is a material that demonstrates several polymorphic phases (*63–73*).

AN, chemically, NH_4NO_3. is typically observed to be a white crystalline solid under standard conditions. Saying that, AN is a polymorphic salt with five different known phase structures observed under certain conditions (*68, 69, 71–76*). The observed phases of AN are designated I through V. Under standard conditions, phase IV is considered the most stable. However, when catalyzing solvents are present, AN can transition from phase IV to phase III. Under standard conditions, phase IV is orthorhombic and has two formula units per cell. Phase III is also orthorhombic, but has four formula units per cell (*69*). Phase transition from IV to III results in swelling of the AN due to a 4% increase in unit cell volume (*77*), and thus an increase in porosity and explosive potential of fertilizer granules. At room temperatures, AN phase IV to III transition can undergo an intermediary very similar to phase II. When phase transitions for AN are observed with Raman, the bands typically associated with symmetric stretch mode of NO_3^- (*21, 78*) shift from phase II at 1050 cm^{-1}, phase III at 1048 cm^{-1}, and phase IV at 1044 cm^{-1}.

There have been several reports in the literature discussing the phase transitions observed in AN and attempts to describe the causes and mechanisms for these transitions. Some results suggest water content and thermal history may play a part in the types of transitions observed; however, some incongruous reports also suggest there might be other factors at play (*6, 7, 21, 22, 24, 63, 64, 67–75, 77, 79, 80*). In 1995, Davey et al. reported that the IV to III transition observed is mainly due to the solubility of AN (*79, 81*). Specifically, they demonstrated that kinetically measured characteristics of the IV to III phase transition are related in magnitude to solution mediated processes like solubility, diffusion, and crystal growth. During the phase transition from IV to III in solution, a disordered interface results when the AN recrystalizes by dissolving and then reforming new domains. This new domain results in an interphase layer that forms at the surface during the nucleation process and interacts with the crystal surface during transition. These interphase layers have been shown to demonstrate distinct and distinguishable Raman signatures (*24, 63, 69*). In other studies of transition mechanisms, it has been suggested that the main differences observed in the transition paths of AN can be attributed to the degree of freedom of the two sets of ions. Specifically, AN ions reorient freely in phases III and II, but in phase IV ions are fixed in orientation. In an article published in 1993, Harju and Valkonen (*80*) reported results studying the effects of cooling and drying times on AN phases observed. They concluded that when samples are cooled slowly, the ions are able to orient themselves in the most energetically favored orientation (phase IV) and therefore form strong bonds. In contrast, when rapid cooling occurs, time for perfect ordering is not achieved and instead disordered crystals (phase III) are observed. Phase IV is characterized as having both ordered nitrate and ammonium ions, III contains ordered nitrate and locally ordered ammonium ions, and phase II contains locally disordered nitrate and ammonium ions. They also concluded that drying moist samples resulted in a phase IV to III dominant transition.

With the considerable examples of different phase transitions being observed dependent on sample treatment methods employed, understanding how real-world sample fabrication processes may impact AN phases produced and ultimately impact standoff hazard detection system evaluations need to be investigated. To investigate this phenomenon, AN was inkjetted onto Klarite and fabricated SERS substrates. The sample phases were determined by collecting SERS spectra from the bands in the 1043–1050 cm^{-1} region that correspond with the symmetric stretch mode of NO_3^- (*21, 78*). From these experiments, some conclusions regarding how substrate type may impact AN phase observed are discussed.

2. Experimental

2.1 Reagents and Materials

AN, methanol, ethanol, and distilled water were obtained from Sigma-Aldrich. All AN inkjet solutions were prepared at various concentrations in solvents of water, methanol, or a mixture of these solvents. All solvents used were high performance liquid chromatography (HPLC) grade. All chemicals were used as received unless otherwise noted.

2.2 SERS Substrates

Commercially available slide mounted standard Klarite (302) SERS substrates were purchased from Renishaw Diagnostics. These substrates consist of a smooth border and a SERS-active patterned grid area. Both surfaces are gold-coated. The Klarite smooth border was used for collecting all Raman measurements, and the patterned grid area for collecting SERS measurements. To protect against environmental and shipping hazards, each substrate is placed in a separate holder enclosed within an opaque vacuum-sealed pouch before shipping. Just prior to use, each substrate was removed from the vacuum-sealed pouch and holder. The substrate was submerged in ethanol to remove any possible contamination that may have accumulated on the surface. Figure 1 shows example scanning electron microscopy (SEM) images of typical standard Klarite SERS substrates. The substrates were used as received. For the purpose of this technical report, overall SERS enhancement is not discussed, instead this substrate is being used to investigate the AN phase response on a SERS surface as compared to the commercially available SERS substrate.

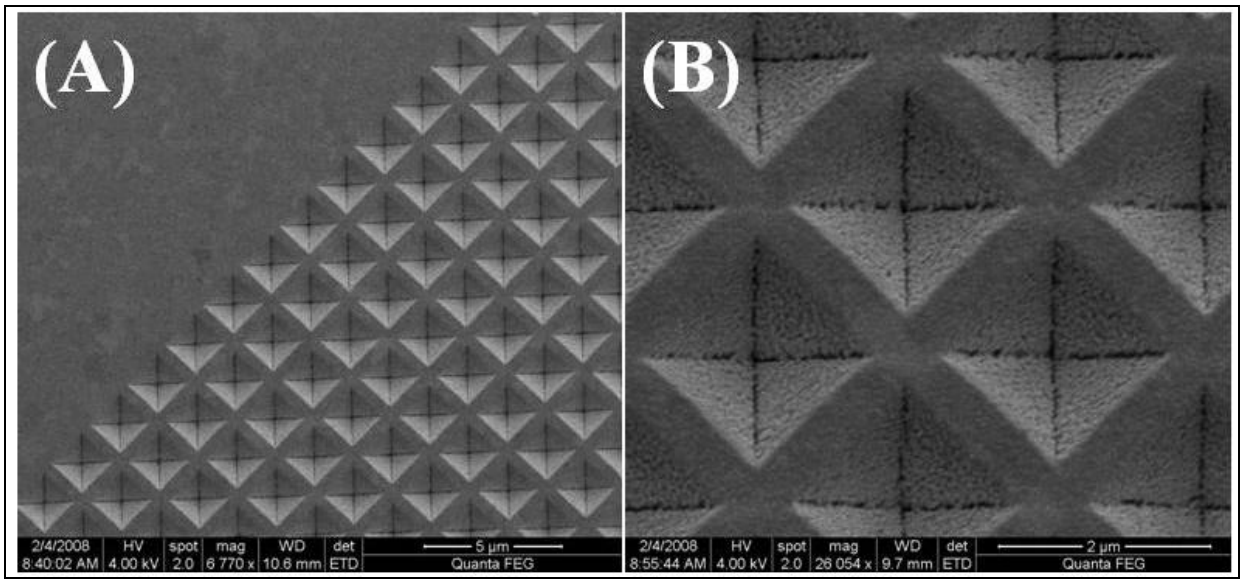

Figure 1. SEM data for the standard Klarite substrate as shown at two different magnifications. In (a) the active area is shown with the features and inactive area appears smooth. In (b) a higher magnification SEM image of the "inverted pyramid" features of the substrate are shown.

2.3 Fabricated SERS Substrates

The samples provided to ARL each contained two 1-mm^2 areas of patterned nanoporous gold (P-NPG). The pattern was fabricated by direct imprinting of porous substrates (DIPS) wherein a silicon stamp is pressed onto the nanoporous gold at a pressure of ~300 N/mm^2. The patterns were designed to efficiently activate surface plasmon resonances without the need to search for hot spots. As mentioned, overall SERS enhancement is not discussed, instead this substrate is being used to investigate the AN phase response on a SERS surface as compared to the fabricated substrate. In figure 2, two microscope images (A and B) are shown at different magnification highlighting the SERS active portion of the substrate, in (C) and (D) SEM images of the actual active area structures are shown at different magnifications.

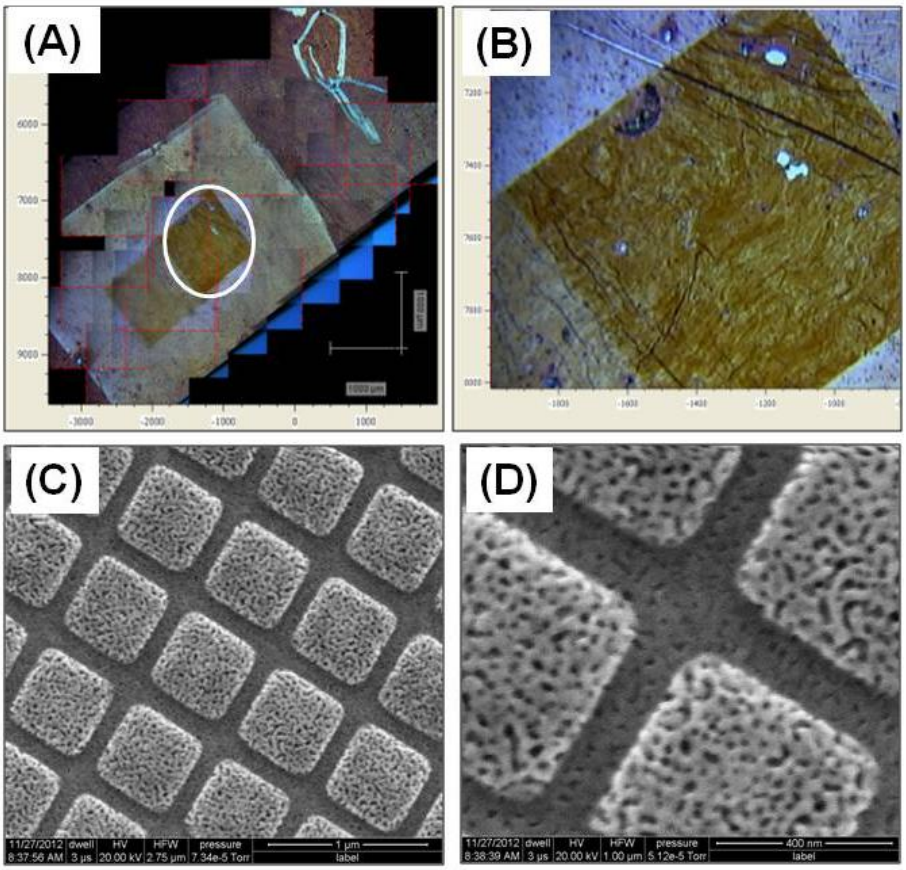

Figure 2. Images of fabricated substrate at different magnifications as viewed through various microscopes. In (a) the SERS active portion of the chip is circled in white as viewed with a microscope. In (b) a larger magnification of the SERS active portion of the substrate is shown as viewed with a microscope. In (c) and (d) the SERS active area of the fabricated substrate is viewed via SEM under increasing magnification.

2.4 Scanning Electron Microscope

SEM images was obtained using a FEI environmental SEM (Quanta 200 FEG).

2.5 SERS Measurements

SERS data were recorded using a Renishaw inVia Reflex Raman microscope equipped with a near-infrared diode laser excitation source ($\lambda = 785$ nm). The light from the diode was focused onto the samples at the microscope stage through a 5× objective. A 5× or 20× objective was used for all measurements unless otherwise noted. Dispersion and resolution of the Renishaw vary with wavelength, but are typically 1 cm^{-1}, decreasing to 0.5 cm^{-1} for certain gratings and wavelengths. Prior to coupling into the microscope, the diode laser beam was circularized by inserting a pinhole into the optical beam path and neutral density filters were used resulting in reduction of the maximum available laser power to 7 mW. Samples at the microscope stage

were positioned remotely with a joystick using an encoded, motorized *XYZ* translation stage (0.1-µm step size) controlled by a Prior Scientific ProScan II controller. WiRE 3.2 software, operating on a bench-top computer, was used for instrument control and data collection. Before all measurements, the instrument was wavelength calibrated using an internal silicon standard. Data analysis was completed using IgorPro 6.0 software (Wavemetrics) (*82*).

2.6 MicroFab Technologies Printer

Materials were produced using a JetLab® 4 (MicroFab Technologies) tabletop printing platform and have been previously documented (*83*). Briefly, the JetLab® 4 is a drop-on-demand inkjet printing system with drop ejection drive electronics (JetDrive™ III), pressure control, a drop visualization system, and precision *X*, *Y*, *Z* motion control (figure 3). The dispensing device (print head assembly, MJ-AL-01-060) consists of a glass capillary tube, with a 60-µm-diameter orifice coupled to a piezoelectric element. Voltage pulses (20–25 V; rise time 1 µs; dwell time 28–32 µs; fall time 1 µs) applied to the piezo result in pressure fluctuations around the capillary. These pressure oscillations propagate through the printing fluid in the tube, resulting in ejection of a microdrop. Drops are visualized using synchronized strobe illumination and a charge-coupled device (CCD) camera. Determining optimal jetting parameters is a trial-and-error process. Stable droplet ejection is achieved by visually observing expelled microdrops and adjusting voltage pulse parameters and capillary fluid backfill pressure. Conditions that provide the highest drop velocity without satellite droplet formation are desired. Printing was performed at a frequency of 250 Hz with a droplet velocity of ~2 m/s. Drop diameter was estimated to be ~60 µm, based on the capillary orifice diameter. During printing, a single substrate was placed on the sample stage. The print head remained fixed at a specified height while the stage moved to print a specified pattern. A rectangular array, which covers a rectangular area with rows of equidistant points, was pre-programmed based on the substrate size and desired sample concentration. An array pattern was chosen for the purpose of creating the effect of a homogeneous coating for optical interrogation. Depending on the desired concentration per unit area (e.g., µg/cm^2), the total number of drops needed to achieve the desired concentration in that area was calculated based on the mass of a single microdrop. Based on the number of total drops needed, the array spacing and drops needed per line can be calculated. These values are easily adjusted depending on concentration. Arrays were printed using the print on-the-fly mode. In this mode, the stage moves continuously as a single microdrop is dispensed at each array element. Print on-the-fly mode improves sample throughput. Fingerprints were also printed from an image and separately calibrated.

Concentrations of deposited materials have been validated using a secondary ultraviolet (UV)-visible (Vis) measurement. This method has been previously documented and typically has R^2 values above 0.998 and relative standard deviations (RSDs) of <3% or better (*83, 84*).

For these experiments, AN was drop-on-demand deposited onto both the commercially available and fabricated SERS substrates at the same time under the same conditions. Therefore, any changes observed in the AN phase structure are directly related to the interactions (chemical or physical) of the AN with the SERS substrate surface and are not attributed to any change/deviations in methodology.

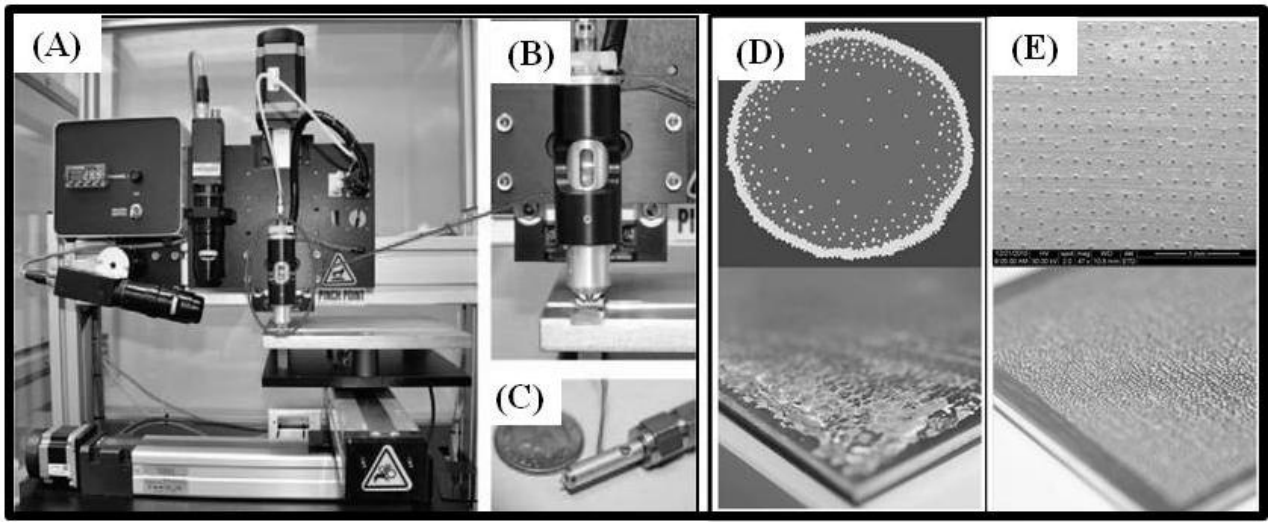

Figure 3 Photographs of (a) JetLab 4 drop-on-demand inkjet printing platform; (b) dispensing device and ink solution encasement; and (c) print head assembly. In (d) graphic and photograph images of drop and dry sample deposition demonstrating coffee ring effect, and in (e) a SEM image and photograph of a microdroplet array demonstrating even sample deposition.

3. Results and Discussion

When inkjetting energetic samples, the desired analyte is suspended in a solvent that is printed and allowed to dry on the coupon surface (drying in a low-heat oven). AN is known to exhibit multiple polymorphic states, therefore understanding the nature of phases fabricated on a printed coupon surface is necessary to better use these reliable test standards in detection system evaluation. To accomplish these goals, a series of experiments were conducted that (1) established the ability to reproducibly print known quantities of sample by effectively calibrating a single droplet of analyte, (2) demonstrated the ability to collect both Raman and SERS data from printed samples, and (3) demonstrated how changes to underlying substrate may impact overall AN phases observed.

3.1 AN Deposition

Accurate deposition of a known concentration of analyte is necessary to ensure the testing standards fabricated are able to properly represent the expected concentration. To determine the

exact mass per drop of the AN deposited onto the SERS substrate, it was first necessary to create and calibrate the mass per droplet jetted into a known volume of solution. To assess the amount of AN in the jetted sample, absorbance measurements were collected. Absorbance measurements were collected using the AN absorbance band located at 303 nm, and collecting an overall peak area. Figure 4a shows a typical absorbance plot. Known numbers of droplets were jetted into solution, and the resulting absorbance measurements collected. From these data, an example calibration curve fabricated from seven measurements is plotted (figure 4b). This calibration plot has a linear fit line matching the equation y=222.28x+0.0043, and an R^2 value of 0.9995 indicating an excellent goodness of fit. From these data, the mass per droplet was found to be approximately 8.31 $x10^{-4}$ µg/drop, with a RSD value of 1.84% between multiple measurements of the same amount deposited. This is a good measure of fit, and we believe any changes in the mass between multiple runs are strictly due to evaporation of the solvent during deposition. Using this technique, the AN solutions of 1.20M, 0.10M, and 0.010M were similarly calibrated (data not shown). From these example calibration curves and others repeated for different analyte solutions (*83*, *84*), ARL has demonstrated a continuous ability to reproducibly and accurately deposit known concentrations of analyte onto surfaces. This ability will aid in the accurate and reproducible fabrication of test panels for the evaluation of hazard detection systems.

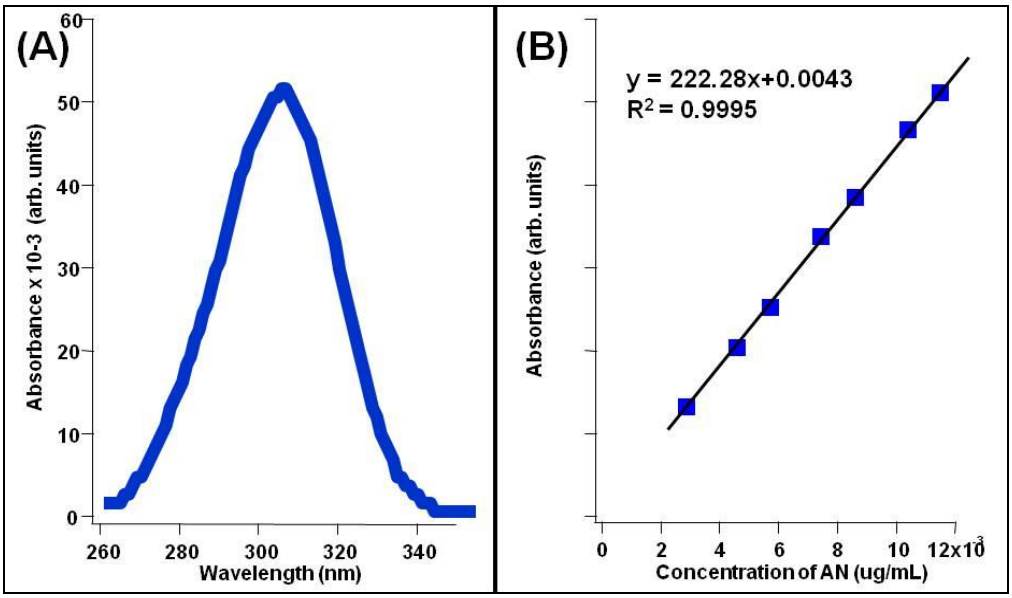

Figure 4. In (a) typical absorbance data for AN demonstrating an absorbance band peak centered at 303 nm is shown, in (b) a calibration curve for AN demonstrating an excellent R^2 value of 0.9995 is shown.

3.2 Characterization of AN Deposition Onto Substrates

Using the jetting system, AN was jetted onto standard Klarite and fabricated SERS substrates. Viewing Klarite samples from a slight angle, it is observed that AN typically forms “dome” shapes across the surface (figure 5). In figure 6, example SEM images of AN jetted onto a Klarite and fabricated SERS substrate are shown. In figure 6a, an example printing of AN across a SERS substrate is shown. The dark spots are the printed AN, the lighter surface area is the SERS active Klarite surface. In this figure, the reproducible and precise spacing of material across the surface is evident in the straight lines of the printed array. In figure 6b, a higher resolution image shows the AN creating a film across the features of the SERS substrate. In figure 6d, the fabricated SERS substrate is shown. This substrate has both active and non-active areas. From figure 6e, AN is observed to set up differently on the non active versus the active surface. In figure 6f, an example of a typical AN droplet on the SERS active surface is shown. When comparing figure 6c and d, the droplet setup on the surfaces is very different. This may in part be due to chemical and/or structural interactions between the analyte and the surface.

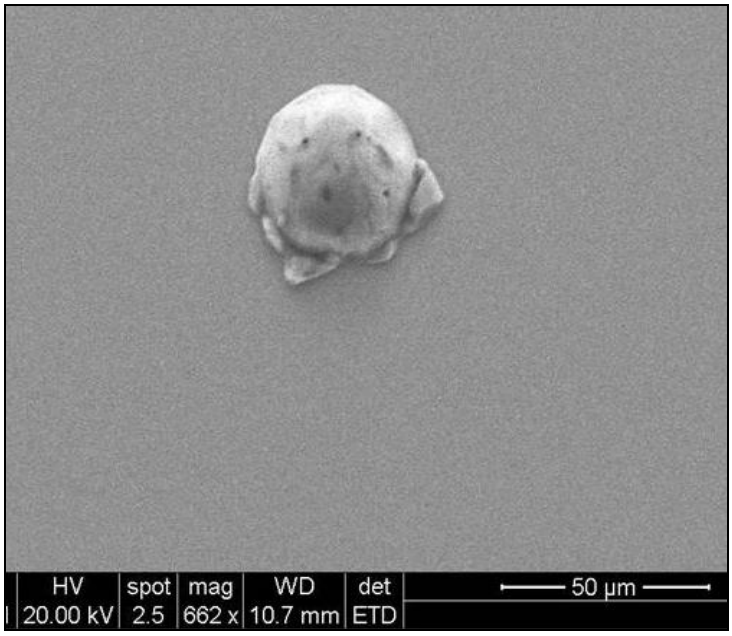

Figure 5. Example SEM image of a typical AN sample as deposited onto a surface. Notice the dome shape of the AN material in this image.

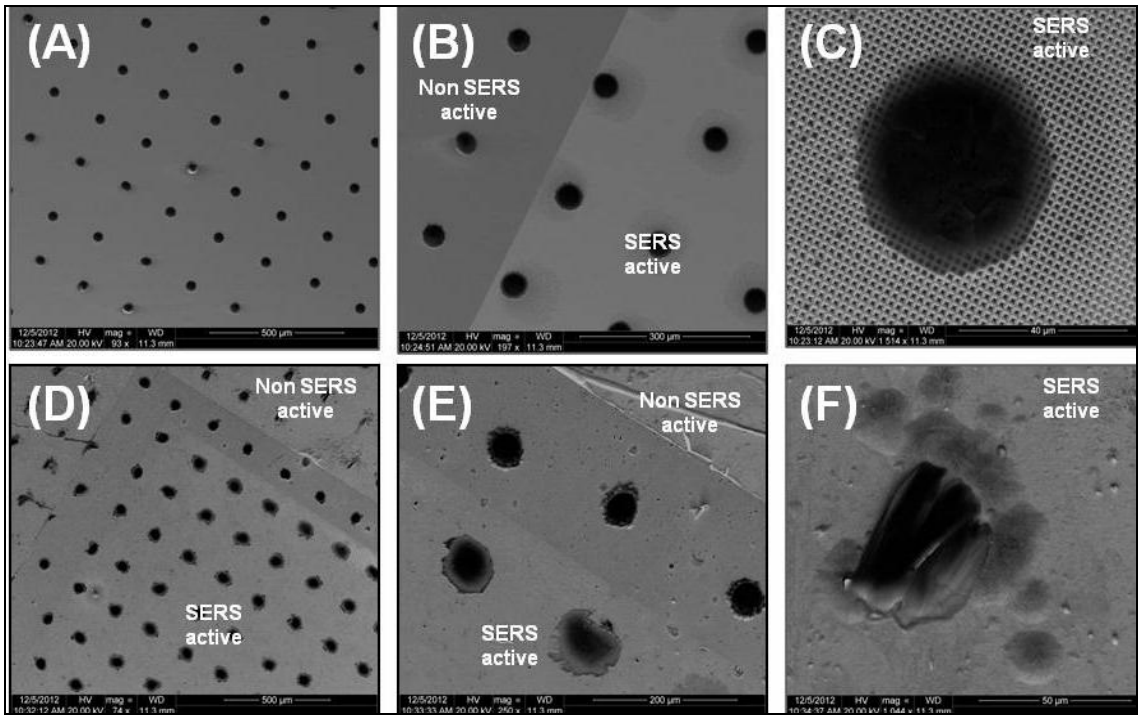

Figure 6. In (a an example printing of AN across a commercially available SERS substrate is shown. The dark spots are the printed AN, the lighter surface area is the SERS active Klarite surface. In (b) the active and non active SERS surface are shown. In (c) a higher resolution image a typical uniform AN droplet across the features of the SERS substrate is shown. In (d) the fabricated SERS substrate is shown. In (e) the SERS active and non SERS active portions of the substrate are shown. The image in (f) shows a single AN droplet across the fabricated substrate.

3.3 Inkjetted Sample Uniformity Characterization

We characterized the uniformity of the printed samples by collecting Raman and SERS spectra from the printed Klarite AN samples. The Klarite substrate was used to determine the uniformity of the printing, because it has been previously shown to be reproducible (structure and overall SERS signal enhancement) batch-to-batch, spot-to-spot, and substrate-to-substrate (*82*). In a typical AN spectrum collected from bulk materials, main Raman and SERS active bands have been reported to be located at or around 713 cm^{-1} and in the 1043 to 1050 cm^{-1} range (NO_3^- stretch mode, phase dependent). According to the literature, at room temperature, AN crystal is expected to be found in the phase IV crystalline polymorph, the most stable AN polymorph, with a main vibrational band for the NO_3^- stretch located at around 1043 cm^{-1}. For these uniformity experiments, AN solutions producing concentrations of 1, 5, and 10 $\mu g/cm^2$ were printed onto a Klarite substrate. To print these different concentration samples, the number of drops deposited at each location was increased; however, all other inkjet system parameters were kept steady (location, spacing between droplets). These concentrations were selected as they represent sample concentrations less than bulk material, but still exhibit enough printed material to "see" an array "haze" across the substrate. The AN samples were deposited and then

allowed to dry in a low temperature (~30 °C; the oven contained desiccant to reduce humidity) oven for 20 min prior to Raman and SERS measurement being collected.

Figure 7a shows an example spectrum from AN printed onto the substrate surface. The main AN band is located at 1048 cm^{-1}. This was not expected because this wavenumber corresponds to the NO_3^- stretch mode observed with phase III of AN. The phase III AN polymorph band was observed with both Raman and SERS data. This reports focuses on SERS data as they resulted in the largest overall signal increase, while exhibiting no change in band location as compared to spontaneous Raman. Recall that the SERS active substrate has small features across it, while the Raman portion of the substrate is a smooth gold surface. For Raman measurements, the smooth surface of the Klarite chip was interrogated, whereas for SERS measurements the patterned grid area of the substrates was used. The same testing instrument parameters/settings were used for all measurements. The data indicated that the AN phase being observed may be partially independent of substrate architecture. From this data, we hypothesize that the sample deposition methodology (ink jetting) might be impacting the polymorphic phases being set up on the substrate surface.

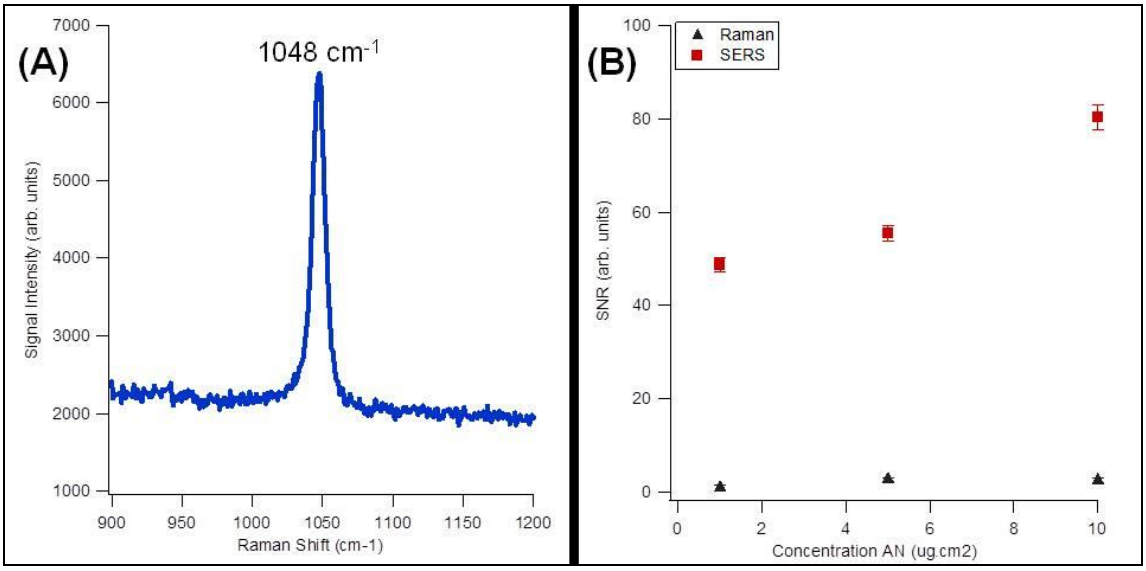

Figure 7. (a) The main AN band located at 1048 cm^{-1} for the SERS and Raman data and (b) S/N ratios for AN deposited at concentrations of 1, 5, and 10 µg/cm^2.

3.4 Polymorphic Phase Change with Sample Concentration

To further investigate how the sample deposition methodology might be impacting the polymorphic phases being set up on the substrate surface as related to sample concentration, spectra from SERS measurements of bulk and non-bulk concentrations of deposited AN on the Klarite substrates were collected. For these experiments, three different solutions of AN with concentrations at 1.20M, 0.10M, and 0.010M were deposited in the same manner across the

substrate surface (location, number of drops, spacing between drops all held constant). Parameters used during printing were such that the final AN deposition concentration was 350.00, 33.50, and 1.7 µg/cm^2 across the surface, respectively. These concentrations were independently validated by UV-Vis measurements (data not shown), and have been previously discussed (*83*). Figure 8a shows examples of the main NO_3^- band located at both 1044 and 1048 cm^{-1}. These data have been normalized for clarity. In figure 8b, focusing on the 1020 to 1070 cm^{-1} spectral region, the shift of the AN band from 1044 cm^{-1} with bulk materials to 1048 cm^{-1} with non-bulk materials is observed. In this figure, the 350 µg/cm^2 sample demonstrates mixed phase characteristics with a main band located at 1044 cm^{-1} and a shoulder at 1048 cm^{-1}. This information is important to note because often for fabricating substrate coupons for field testing, numerous concentrations ranging from bulk to trace are used. If different polymorphic phases are being observed, it is necessary to ensure that accurate spectral libraries are created that have information from many different concentration ranges. Having observed polymorphic phases in printed bulk and higher concentration AN, we were curious how trace quantities of printed AN may behave.

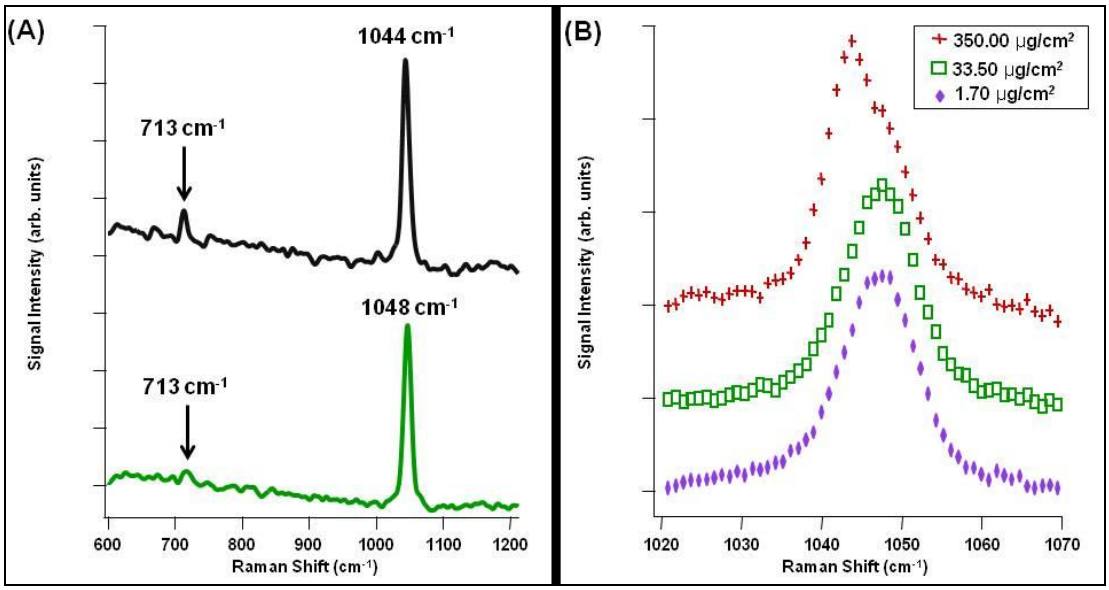

Figure 8. (a) An example of shifting main AN NO_3^- band (normalized) and (b) several example SERS spectrum from ammonium nitrate at varying concentrations as collected on the Klarite substrate. The location of the main AN bands changes, indicating a difference in phase with a change in material concentration from bulk to non-bulk material.

3.5 AN Polymorphic Phase Change Observed with Substrate Variation

Having characterized a change in AN phase with concentration, we next looked at how the surface of the Raman/SERS substrate may impact the phases being observed. For these experiments, AN was inkjetted onto the Klarite SERS substrate and the fabricated SERS substrate following the same conditions at the same time. The AN was jetted at a 25 µg/cm^2

concentration onto the substrate surface. Figure 9 shows the Raman and SERS data as collected from the Klarite and fabricated SERS substrate. (For the purpose of this report, no discussion of actual SERS enhancement is discussed, instead the reader should focus on the interesting change in phases as observed with the different substrates.) In figure 9a and b, the SERS and Raman data on the Klarite display a main AN band located at 1048 cm^{-1}, corresponding with AN phase III. Figure 9b and c shows the SERS and Raman data, respectively, on the fabricated SERS substrate. The AN band for the fabricated SERS substrate is located at 1044 cm^{-1}, corresponding with phase IV AN. Understanding that AN can display different phases depending on the underlying material is necessary when training and evaluating standoff hazard detection systems. This is also of interest because it suggests that material preparation is not the only aspect that can impact the overall AN phase observed.

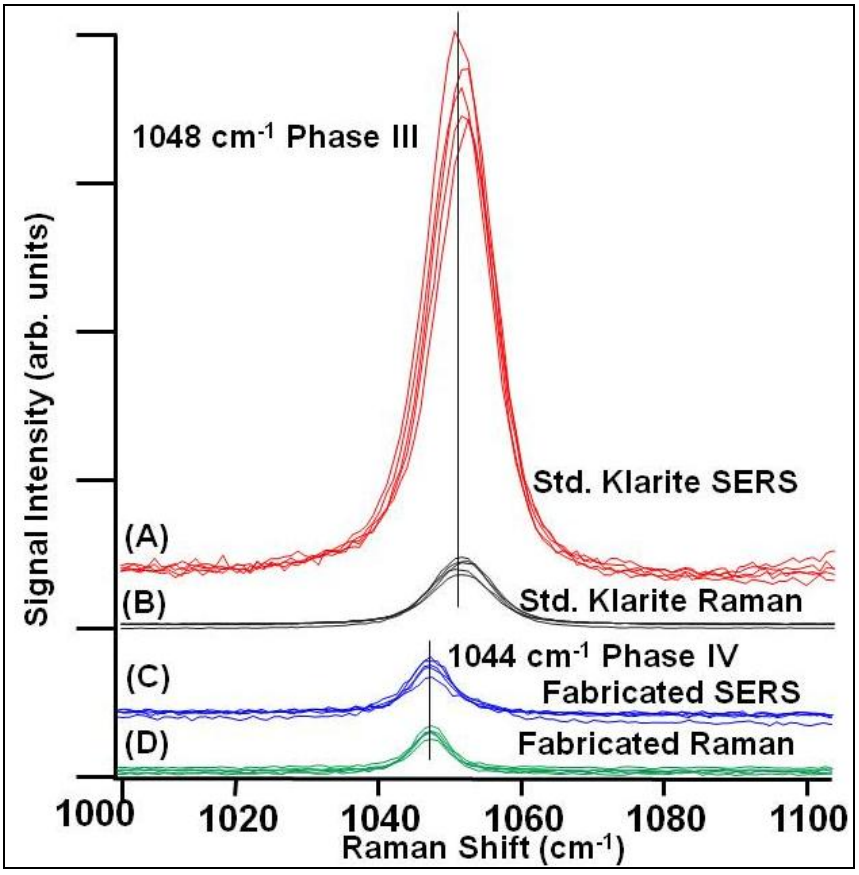

Figure. 9. SERS and Raman spectra from AN sample inkjetted onto substrates. The Klarite (a) SERS and (b) Raman response is shown with a main AN band located at 1048 cm^{-1}. The fabricated substrate has (c) SERS and (d) Raman bands located at 1044 cm^{-1}. The difference in band location may in part be attributed to physical and chemical interactions between the AN and the surface.

4. Conclusions

When fabricating samples for evaluating optical detection technologies using a drop-on-demand inkjet system, the potential to fabricate samples containing multiple polymorphic phases must be considered. This is vital, because a hazard detection system must be accurately ‘‘trained’’ if it is to detect and identify multiple polymorphic states of materials based on spectral features, thus accurately differentiating between hazardous and benign unknowns.

In this report, the impact of deposited AN at various concentrations and onto different substrate bases was investigated. From these efforts, we have made some interesting observations. First, the concentration of material deposited seems to impact the AN polymorphic phase observed. Specifically, this was demonstrated when AN was deposited onto a commercial Klarite substrate at concentrations of 350 and 1.7 μg/cm^2—the former demonstrated the phase IV polymorph while the latter exhibited phase III. In this work, we also observed that deposited the same concentration of material onto different substrate architectures (commercial and fabricated SERS substrates) also impacts the AN phase (perhaps due to structural and chemical interactions).

Based on this work, we will continue to investigate the influence of substrate handling, sample preparation methods, and substrate material on energetic sample phases. To achieve this goal, we are looking at pure AN on several substrate types including metals, plastics, cloth, and biological samples at various concentrations. We also intend to investigate if different vendors/sources of AN may influence the phases observed in jetted materials.

Understanding how energetic material samples interact with many common factors (material, environmental conditions, even concentration) may lead to a better ability to fabricate real-world sample materials, result in a more accurate training and evaluation of standoff hazard detection systems, and ultimately, improve the ability to keep U.S. Army and other military personal protected.

5. References

1. Wikipedia. “Oklahoma City bombing”. 2012. http://en.wikipedia.org/wiki/Oklahoma_City_bombing (accessed 28 January 2013).
2. “IED attacks in Afghanistan set record”. 2012. http://www.usatoday.com/news/world/story/2012-01-25/IEDs-afghanistan/52795302/1 (accessed January 26, 2012).
3. Sanders, K. P.; Marshall, M.; Oxley, J.; Smith, J. L.; Egee, L. Preliminary Investigation into the Recovery of Explosives From Hair. *Sci. Just.* **2002**, *42* (3), 137–142.
4. Oxley, J.; Smith, J.; Brady, J.; Dubnikova, F.; Kosloff, R.; Zeiri, L.; Zeiri, Y. Raman and Infrared Fingerprint Spectroscopy of Peroxide-based Wxplosives. *Appl. Spec.* **2008**, *62* (8), 906–915.
5. Gregory, O.; Oxley, J.; Smith, J.; Platek, M.; Ghonem, H.; Bernier, E.; Downey, M.; Cumminskey, C. Sensors Surface Technology, P. Microstructural Characterization of Pipe Bomb Fragments. *Mater. Charact.* **2010**, *61* (3), 347–354.
6. Oxley, J.; Smith, J. L.; Brady, J.; Naik, S. Determination of Urea Nitrate and Guanidine Nitrate Vapor Pressures by Isothermal Thermogravimetry. *Prop. Explos. Pyro.* **2010**, *35* (3), 278–283.
7. De Perre, C.; Prado, A.; McCord, B. R. Rapid and Specific Detection of Urea Nitrate and Ammonium nitrate by Electrospray Ionization Time-of-flight Mass Spectrometry Using Infusion with Crown Ethers. *Rapid Communications in Mass Spectrometry* **2012**, *26* (2), 154–162.
8. Natan, A.; Levitt, J. M.; Graham, L.; Katz, O.; Silberberg, Y. Standoff Detection via Single-beam Spectral Notch Filtered Pulses. *Appl. Phys. Lett.* **2012**, *100* (5), 051111.
9. Ramin, S.; Weller, M. G. Extremely Sensitive and Selective Antibodies Against the Explosive 2,4,6-trinitrotoluene by Tational Design of a Structurally Optimized Hapten. *J. Mol. Recog.* **2012**, *25* (2), 89–97.
10. Upadhyayula, V.K.K. Functionalized Gold Nanoparticle Supported Sensory Mechanisms Applied in Detection of Chemical and Biological Threat Agents: A Review. *Anal. Chim. Acta.* **2012**, (715), 1–18.

11. Wen, B.; Eilers, H. Potential Interference Mechanism for the Detection of Explosives via Laser-based Standoff Techniques. *Applied Physics B-Lasers and Optics.* **2012**, *106* (2), 473–482.

12. Wallin, S.; Pettersson, A.; Ostmark, H.; Hobro, A. Laser-based Standoff Detection of Explosives: A Critical Veview. *Anal. Bioanal. Chem.* **2009**, *395* (2), 259–274.

13. Zachhuber, B.; Ramer, G.; Hobro, A.; Chrysostom, E.T H.; Lendl, B. Stand-off Raman Spectroscopy: A Powerful Technique for Qualitative and Quantitative Analysis of Inorganic and Organic Compounds Including Explosives. *Analytical and Bioanalytical Chemistry.* **2011**, *400* (8), 2439–2447.

14. Fulton, J. Remote Detection of Explosives Using Raman Spectroscopy, In *Chemical, Biological, Radiological, Nuclear, and Explosives* (Fountain, A. W. and Gardner, P. J., Eds.), 2011.

15. Loeffen, P. W.; Maskall, G.; Bonthron, S.; Bloomfield, M.; Tombling, C.; Matousek, P. Chemical and Explosives Point Detection Through Opaque Containers Using Spatially Offset Raman Spectroscopy (SORS), In *Chemical, Biological, Radiological, Nuclear, and Explosives* (Fountain, A. W. and Gardner, P. J., Eds.), 2011.

16. Emmons, E. D.; Farrell, M. E.; Holthoff, E. L.; Tripathi, A.; Green, N.; Moon, R. P.; Guicheteau, J. A.; Christesen, S. D.; Pellegrino, P. M.; Fountain, A. W., III. Characterization of Polymorphic States in Energetic Samples of 1,3,5-Trinitro-1,3,5-Triazine (RDX) Fabricated Using Drop-on-Demand Inkjet Technology. *Appl. Spec.* **2012**, *66* (6), 628–635.

17. Emmons, E. D.; Guicheteau, J. A.; Fountain, A. W., III; Christesen, S. D. Comparison of Visible and Near-Infrared Raman Cross-Sections of Explosives in Solution and in the Solid State. *Appl. Spec.* **2012**, *66* (6), 636–643.

18. Ghosh, M.; Wang, L.; Asher, S. A. Deep-Ultraviolet Resonance Raman Excitation Profiles of NH4NO3, PETN, TNT, HMX, and RDX. *Appl. Spec.* **2012**, *66* (9), 1013–1021.

19. Izake, E. L. Forensic and Homeland Security Applications of Modern Portable Raman Spectroscopy. *Foren. Sci. Int.* **2010**, *202* (1), 1–8.

20. Scaffidi, J. P.; Gregas, M. K.; Lauly, B.; Carter, J. C.; Angel, S. M.; Vo-Dinh, T. Trace Molecular Detection via Surface-Enhanced Raman Scattering and Surface-Enhanced Resonance Raman Scattering at a Distance of 15 Meters. *Appl. Spec.* **2010**, *64* (5), 485–492.

21. Tuschel, D. D.; Mikhonin, A. V.; Lemoff, B. E.; Asher, S. A. Deep Ultraviolet Resonance Raman Excitation Enables Explosives Detection. *Appl. Spec.* **2010**, *64* (4), 425–432.

22. Ostmark, H.; Nordberg, M.; Carlsson, T. E. Stand-off Detection of Explosives Particles by Multispectral Imaging Raman Spectroscopy. *App. Optic.* **2011**, *50* (28), 5592–5599.

23. Zachhuber, B.; Gasser, C.; Chrysostom, E.T.H.; Lendl, B. Stand-Off Spatial Offset Raman Spectroscopy for the Detection of Concealed Content in Distant Objects. *Anal. Chem.* **2011**, *83* (24), 9438–9442.

24. Zachhuber, B.; Ramer, G.; Hobro, A.; Chrysostom, E.T.H.; Lendl, B. Stand-off Raman Spectroscopy: A Powerful Technique for Qualitative and Quantitative Analysis of Inorganic and Organic Compounds Including Explosives. *Anal. Bioanal. Chem.* **2011,** *400* (8), 2439–2447.

25. Piorek, B. D.; Lee, S. J.; Moskovits, M.; Meinhart, C. D. Free-Surface Microfluidics/Surface-Enhanced Raman Spectroscopy for Real-Time Trace Vapor Detection of Explosives. *Analytical Chemistry.* **2012**, *84* (22), 9700–9705.

26. Farrell, M. E.; Holthoff, E. L.; Pellegrino, P. M. Next Generation Surface Enhanced Raman Scattering (SERS) Substrates for Hazard Detection, In *Chemical, Biological, Radiological, Nuclear, and Explosives* (Fountain, A. W., Ed.), 2012.

27. Chou, A.; Jaatinen, E.; Buividas, R.; Seniutinas, G.; Juodkazis, S.; Izake, E. L.; Fredericks, P. M. SERS Substrate for Detection of Explosives. *Nanoscale* **2012**, *4* (23), 7419–7424.

28. Bantz, K. C.; Meyer, A. F.; Wittenberg, N. J.; Im, H.; Kurtulus, O.; Lee, S. H.; Lindquist, N. C.; Oh, S. H.; Haynes, C. L. Recent Progress in SERS Biosensing. *Phy. Chem. Chem. Phy*. **2011**, *13* (24), 11551–11567.

29. Abdelhamid, M.; Fortes, F. J.; Harith, M. A.; Laserna, J. J. Analysis of Explosive Residues in Human Fingerprints Using Optical Catapulting-laser-induced Breakdown Spectroscopy. *J. Anal. Atom. Spectro.* **2011**, *26* (7), 1445–1450.

30. Banas, A.; Banas, K.; Breese, M.B.H.; Loke, J.; Teo, B. H.; Lim, S. K. Detection of Microscopic Particles Present as Vontaminants in Latent Gingerprints by Means of Dynchrotron Tadiation-based Fourier Yransform Infra-red Micro-imaging. *Analyst.* **2012**, *137* (15), 3459–3465.

31. Cullum, H. E.; McGavigan, C.; Uttley, C. Z.; Stroud, M.A.M.; Warren, D. C. A Second Survey of High Explosives Traces in Public Places. *J. Foren. Sci.* **2004**, *49* (4), 684–690.

32. Docherty, F. T.; Monaghan, P. B.; McHugh, C. J.; Graham, D.; Smith, W. E.; Cooper, J. M. Simultaneous Multianalyte Identification of Molecular Species Involved in Terrorism Using Raman Spectroscopy. *IEEE Sens. J.* **2005**, *5* (4), 632–640.

33. Emmons, E. D.; Tripathi, A.; Guicheteau, J. A.; Christesen, S. D.; Fountain, A. W., III. Raman Chemical Imaging of Explosive-Contaminated Fingerprints. *Appl. Spec.* **2009**. *63* (11), 1197–1203.

34. Hazarika, P.; Russell, D. A. Advances in Fingerprint Analysis. *Ange. Chemie-Intern. Ed.* **2012**, *51* (15), 3524–3531.

35. Guicheteau, J.; Christesen, S.; Tripathi, A.; Emmons, E.; Emge, D.; Wilcox, P.; Fountain, A. W., III. Raman and Surface-enhanced Raman for Military Applications. A*IP Conf. Proc.* **2010**, 1267.

36. Hankus, M. E.; Stratis-Cullum, D. N.; Pellegrino, P. M. Towards Advanced Biological Detection using Surface Enhanced Raman Scattering (SERS)-based Sensors. *SPIE.* **2010**, 7759.

37. Holthoff, E. L.; Stratis-Cullum, D. N.; Hankus, M. E. A Nanosensor for TNT Detection Based on Molecularly Imprinted Polymers and Surface Enhanced Raman Scattering. *Sensors* **2011**, *11* (3), 2700–2714.

38. Fleischmann, M.; Hendra, P. J.; McQuillan, A. J. *Chem. Phys.Lett.* **1974**, *26*, 163–166.

39. Jeanmaire, D. L.; Vanduyne, R. P. Surface Raman Spectroelectrochemistry Heterocyclic, Aromatic, and Aliphatic-Amines Adsorbed on Anodized Silver Electrode. *J. Electroanal. Chem.* **1977**, *84* (1), 1–20.

40. Albrecht, M. G.; Creighton, J. A. Anomalously Intense Raman-Spectra of Pyridine at a Silver Electrode. *J. Am. Chem. Soc.* **1977**, *99* (15), 5215–5217.

41. Kneipp, K.; Kneipp, H.; Dasari, R. R.; Feld, M. S. Single Molecule Raman Spectroscopy Using Silver and Gold Nanoparticles. *Indian J. Phys. Proc. Indian Assoc. Cultiv. Sci. B.* **2003**, *77B* (1), 39–47.

42. Cotton, T. M.; Kim, J. H.; Chumanov, G. D. Application of Surface-enhanced Raman Spectroscopy to Biological Systems. *J. Raman Spectro.* **1991**, *22* (12), 729–742.

43. Campion, A.; Kambhampati, P. Surface-enhanced Raman Scattering. *Chem. Soc. Rev.* **1998**, *27* (4), 241–250.

44. Kneipp, K.; Kneipp, H.; Itzkan, I.; Dasari, R. R.; Feld, M. S. Surface-enhanced Raman Scattering and Biophysics. *Journal of Physics-Condensed Matter.* **2002**, *14* (18), R597–R624.

45. Baker, G. A.; Moore, D. S. Progress in Plasmonic Engineering of Surface-enhanced Raman-Scattering Substrates Toward Ultra-trace Analysis. *Anal. Bioanal. Chem.* **2005**, *382* (8), 1751–1770.

46. Yonzon, C. R.; Stuart, D. A.; Zhang, X. Y.; McFarland, A. D.; Haynes, C. L.; Van Duyne, R. P. Towards Advanced Vhemical and Niological Nanosensors - An Overview. *Talanta.* **2005**, *67* (3), 438–448.

47. Willets, K. A.; Van Duyne, R. P. Localized Surface Plasmon Resonance Spectroscopy and Sensing. **2007**, *58*.

48. Banholzer, M. J.; Millstone, J. E.; Qin, L. D.; Mirkin, C. A. Rationally Designed Nanostructures for Surface-enhanced Raman Spectroscopy. *Chem. Soc. Rev.* **2008**, *37* (5), 885–897.

49. Kneipp, J.; Kneipp, H.; Kneipp, K. SERS - A Single-molecule and Nnanoscale Tool for Bioanalytics. *Chem. Soc. Rev.* **2008**, *37* (5), 1052–1060.

50. Qian, X. M.; Nie, S. M. Single-molecule and Single-nanoparticle SERS: from Fundamental Mechanisms to Biomedical Applications. *Chem. Soc. Rev.* **2008**, *37* (5), 912–920.

51. Stiles, P. L.; Dieringer, J. A.; Shah, N. C.; Van Duyne, R. R. Surface-Enhanced Raman Spectroscopy, In *Annual Review of Analytical Chemistry*, pp 601–626, 2008.

52. Ryckman, J. D.; Liscidini, M.; Sipe, J. E.; Weiss, S. M. Direct Imprinting of Porous Substrates: A Rapid and Low-Cost Approach for Patterning Porous Nanomaterials. *Nano Letters.* **2011**, *11* (5), 1857–1862.

53. Yang, J.; Ryckman, J. D.; Ciesielski, P. N.; Escobar, C. A.; Jennings, G. K.; Weiss, S. M. Patterned Nanoporous Gold as an Effective SERS Template. *Nanotechnology* **2011**, *22* (29), 295302 (295306 pp.)–295302 (295306 pp.).

54. Jiao, Y.; Ryckman, J. D.; Ciesielski, P. N.; Escobar, C. A.; Jennings, G. K.; Weiss, S. M. Patterned Nanoporous Gold as an Effective SERS Template. *Nanotechnology* **2011**, *22* (29).

55. Alexander, T. A. Applications of Surface-Enhanced Raman Spectroscopy (SERS) for Biosensing: An Analysis of Reproducible, Commercially Available Substrates. *SPIE.* **2005**, *6007*, 600703.

56. Alexander, T. A. Development of Methodology Based on Commercialized SERS-active Susbtrates for Rapid Discrimination of Poxviridae Virions. *Anal. Chem.* **2008**, *80* (8), 2817–2825.

57. Alexander, T. A.; Le, D. M. Characterization of a Commercialized SERS-active Substrate and its Application to the Identification of Intact Bacillus Endospores. *Appl. Opt.* **2007**, *46* (18), 3878–3890.

58. Alexander, T. A.; Pellegrino, P. M.; Gillespie, J. B. Near-infrared Surface-enhanced-Raman-scattering-mediated Detection of Single Optically Trapped Bacterial Spores. *Appl. Spec.* **2003**, *57* (11), 1340–1345.

59. Netti, M. C.; Zoorob, M. E.; Charlton, M.C.B.; Ayliffe, P.; Mahnkopf, S.; Stopford, P.; Todd, K.; Lincoln, J. R.; Perney, N.M.B.; Baumberg, J. J. Probing Molecules by Surface-enhanced Raman Spectroscopy. *SPIE* **2006**, *6093*.

60. Hankus, M.; Stratis-Cullum, D.; Pellegrino, P. *Enabling Technologies for Point and Remote Sensing of Chemical and Biological Agents Using Surface Enhanced Raman Scattering (SERS) Techniques*; ARL-TR-4957; U.S. Army Research Laboratory: Adelphi, MD, 2009.

61. Emmons, E. D.; Farrell, M. E.; Holthoff, E. L.; Tripanthi, A.; Green, N.; Moon, R. P.; Guicheateau, J. A.; Christesen, S.; Pellegrino, P. M.; Fountain III, A. W. Characterization of Polymorphic States in Energetic Samples of 1,3,5-Trinitro-1,3,5-Triazine (RDX) Fabricated Using Drop-on-Demand Inkjet Technology. *Appl Spectrosc.* **2012**, *66* (6). 628–635

62. Capes, J. S.; Cameron, R. E. Contact Line Crystallization to Obtain Metastable Polymorphs. *Cryst. Growth Des.* **2007**, *7* (1), 108–112.

63. Kettle, S. The Raman Spectra of Phase III Ammonium Nitrate, p 17, Air Force Office of Scientific Research (AFSC) USAF.

64. Harju, M.E.E. Solid State Transition Mechanisms of Ammonium-nitrate Phase-IV, Phase III and Phase II Investigated by Simultaneous Raman-spectrometry and Differential Scanning Calorimetry. *Appl. Spectros.* **1993**, *47* (11), 1926–1930.

65. James, D. W.; Carrick, M. T.; Leong, W. H. Structural Studies of Ammonium Nitrate - Phases III, IV, and V. *Chemical Physics Letters.* **1974**, *28* (1), 117–119.

66. Holden, J. R.; Dickinson, C. W. Crystal Structure of 2 Solid Solution Phases of Ammonium Nitrate and Pottasium Nitrate. *Journal of Physical Chemistry* **1975**, *79* (3), 249–256.

67. Choi, C. S.; Mapes, J. E.; Prince, E. Structure of Ammonium Nitrate (IV). *Acta Crystal. Sect. B-Struct. Cryst. Cryst.Chem.* **1972**, *28* (5), 1357.

68. Brown, R. N.; McLaren, A. C. On Mechanism of Thermal Transformations in Solid Ammonium Nitrate. *P. Roy. Soc. Lond. A Mat.* **1962**, *266* (1326), 329.

69. Akiyama, K.; Morioka, Y.; Nakagawa, I. Raman Scattering and PhaseTransition of Ammonium Nitrates. *Bulletin of the Chemical Society of Japan.* **1981**, *54* (6), 1662–1666.

70. Davey, R. J.; Ruddick, A. J.; Guy, P. D.; Mitchell, B.; Maginn, S. J.; Polywka, L. A. The IV-III Polymorphic Phase-transition in Smmonium Nitrate – A Unique Example of Solvent Mediation. *J. Phys. D. Apply. Phys.* **1991**, *24* (2), 176–185.

71. Vargeese, A. A.; Joshi, S. S.; Krishnamurthy, V. N. Effect of Method of Crystallization on the IV-III and IV-II Polymorphic Transitions of Ammonium Nitrate. *J. Hazard. Mater.* **2009**, *161* (1), 373–379.

72. Chien, W. M.; Chandra, D.; Lau, K. H.; Hildenbrand, D. L.; Helmy, A. M. The Vaporization of NH(4)NO(3). *J.Chem. Thermo.* **2010**, *42* (7), 846–851.

73. Kim, J. K.; Choi, S. I.; Kim, E. J.; Kim, J. H.; Koo, K. K. Preparation of Spherical Ammonium Nitrate Particles by Melt Spray. *Industrial & Engineering Chemistry Research* **2010**, *49* (24), 12632–12637.

74. Wu, H. B.; Chan, M. N.; Chan, C. K. FTIR Characterization of Polymorphic Transformation of Ammonium Nitrate. *Aerosol Science and Technology* **2007**, *41* (6), 581–588.

75. Savara, A.; Li, M. J.; Sachtler, W.M.H.; Weitz, E. Catalytic Reduction of NH4NO3 by NO: Effects of Solid Acids and Implications for Low Temperature DeNO(x) Processes. *Applied Catalysis B-Environmental* **2008**, *81* (3–4), 251–257.

76. Nasirov, E. V.; Asadov, Y. G. Kinetics of the II -> III Polymorphic Transformation in KNO(3)-RbNO(3) Solid Solutions. *Inorganic Materials* **2010**, *46* (8), 885–888.

77. Vogels, L.J.P.; Bennema, P.; Hottenhuis, M.H.J.; Elwespoek, M. C. On the Morphology of Smmonium Nitrate (III): Theory and Observation. *J. Crys. Grow.* **1991**, *108*, 733–743.

78. Owens, F. J. Reproducible Surface-enhanced Raman Spectroscopy of Small Molecular Anions. *Mol. Phys.* **2011**, *109* (5), 667–671.

79. Davey, R. J.; Ruddick, A. J.; Guy, P. D.; Mitchell, B.; Maginn, S. J.; Ploywka, L. A. The IV-III Polymorphic Phase Transition in Ammonium Nitrate: A UniqueExample of Solvent Mediation. *J. Phys. D. Apply. Phys.* **1991**, *24*, 176–185.

80. Harju, M E E.; Valonen, J. Effect of Sample Treatment on the Phase Transition Paths of Ammonium Nitrate Solid State Phases IV, III, and II. *J.Therm. Anal.* **1993**, *39*, 681–693.

81. Davey, R. J.; Guy, P. D.; Ruddick, A. J. The IV- III Polymophic Phase Transition in Aqueous Slurries of Ammonium Nitrate. *J.Col. Interf. Sci.* **1985**, *108* (1), 189–192.

82. Hankus, M. E.; Stratis-Cullum, D. N.; Pellegrino, P. M. Characterization of Next-generation Commercial Surface-enhanced RamanScattering (SERS) Substrate. *SPIE.* **2011**, *8018*, 80180P.

83. Holthoff, E. L.; Hankus, M. E.; Pellegrino, P. M. Investigating a Drop-on-Demand Microdispenser for Standardized Sample Preparation. *SPIE*. **2011**, *8018*, 80181F–80190F.

84. Holthoff, E. L.; Farrell, M. E.; Pellegrino , P. M. Investigating a Drop-on-Demand Microdispenser for Standardized Sample Preparation. *SPIE.* **2012**, *8358*.

List of Symbols, Abbreviations, and Acronyms

AN	ammonium nitrate
ARL	U.S. Army Research Laboratory
ARO	U.S. Army Research office
CCD	charge-coupled device
DIPS	direct imprinting of porous substrates
HME	Homemade explosive
HPLC	high performance liquid chromatography
IED	improvised explosive device
PECASE	Presidential Early Center Award for Scientists and Engineers
P-NPG	patterned nanoporous gold
RSD	relative standard deviation
SEM	scanning electron microscope
SERS	surface enhanced Raman scattering
UV	ultraviolet
VIS	visible

NO. OF COPIES	ORGANIZATION
1 ELEC	ADMNSTR DEFNS TECHL INFO CTR ATTN DTIC OCP
1 PDF	MIKELLA FARRELL U.S. ARMY RESEARCH LABORATORY RDRL-SEE-O
1 PDF	GARY WOOD U.S. ARMY RESEARCH LABORATORY RDRL-SEE
1 PDF	LINDA BLISS U.S. ARMY RESEARCH LABORATORY RDRL-SEE
1 PDF	US ARMY RSRCH LAB ATTN RDRL CIO LL TECHL LIB ADELPHI MD 20783-1197

INTENTIONALLY LEFT BLANK.